Failure Mechanisms of Aluminum Bondpad Peeling During Thermosonic Bonding

Cher Ming Tan, *Senior Member, IEEE,* and Zhenghao Gan

***Abstract*—Aluminum bondpad peeling was observed in a newly developed thermosonic wirebonding process for chip-on-board assembly. Through detailed failure analysis and with the help of finite element analysis on stress simulation, the true root cause of the peeling is identified. It is found that the true root cause is the effect of skidding force as a result of the constrained movement of the bonding tool as bonding is done on a chip assembled in a plastic casing. With a change in the bonding tool movement, the peeling phenomenon is completely eliminated.**

***Index Terms*—Bondpad peeling, confocal microscope, failure mechanism, finite element analysis, skidding, thermosonic bonding.**

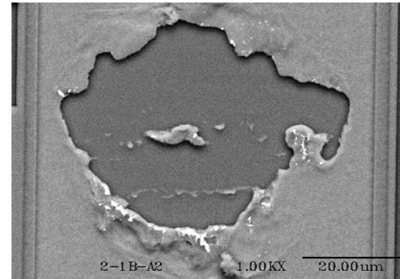

Fig. 1. SEM micrograph of bondpad with ABPO.

I. Introduction

Wire bonding is still the dominant form of interconnection from chip to the external world. While the wirebond failure rate for individually packaged parts is in the low parts per million [1], the failure rates for wirebonds in multichip modules (MCMs) and chip-on-board (COB) assemblies remain high [2].

A thermosonic wire bonding process is developed for the wire bonding on chips assembled in a plastic casing. The bonding temperature is lowered to 115 °C as the casing cannot withstand high temperature. Hu *et al.* [3] have shown that for thermosonic bonding of Au wire to Al bondpad, bondability can be achieved for the temperature range of 110–160 °C. Also, because of the limited space for the bonding tool to move around within the plastic casing, the movement of the bonding tool is modified from the standard bonding process.

However, with such a new process, serious fallout was found due to the aluminum bondpad peel off (ABPO) from the chip as shown in Fig. 1. The peel off occurred immediately after the bonding process, and the percentage of fallout can go beyond 10% in some cases.

In this paper, we will examine the root cause of the ABPO. Known failure mechanisms that result in similar failure mode will be reviewed first, and possible root causes will be identified. Finite element analysis will be performed to find the true root cause(s) among the possible causes.

II. Failure Analysis of ABPO and Possible Failure Mechanisms

Failure analysis was performed on the fallout. The bondpad consists of top metal layer of Al deposited on $MoSi_2$. The $MoSi_2$

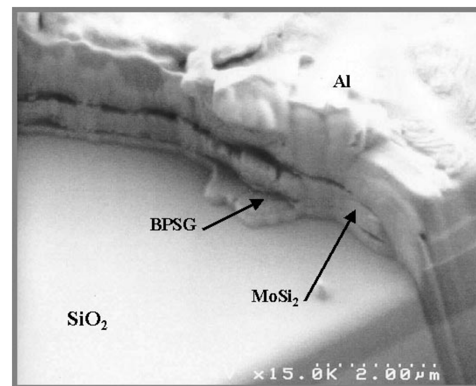

Fig. 2. Closer SEM micrograph of the peeled section of a bondpad.

is the results of silicidation of Mo and the underlying borophosphorosilicate glass (BPSG) layer that is deposited on top of the SiO_2 as shown in Fig. 2. One can easily identify the four layers using energy dispersive spectroscopy (EDS) analysis. The scanning electron microscopy (SEM) micrograph in Fig. 2 clearly showed that the peel off occurred at the BPSG/SiO_2 interface.

It was also found that for chips with ABPO, the bond shear forces of nonpeeled-off pads on the same dies are well within the specifications. In fact, no correlation was found between the bond shear strength and the percentage of ABPO. Hence, the root cause of ABPO is unlikely to be those that cause poor shear force.

Therefore, the peeling is most likely due to either cratering or excessive stress in the BPSG film. Chen *et al.* [4] used a fractional factorial-designed experiment to study the effect of bonding parameters on cratering for the thermosonic Au ball bonding. They found that the three most important bonding parameters are the bonding power, bonding force, and temperature. Clatterbaugh *et al.* [5] also performed an extensive study on the cratering. They found that cratering is more significant when

Manuscript received October 9, 2002; revised April 17, 2003.

The authors are with the School of Electrical and Electronic Engineering, Nanyang Technological University, 639798 Singapore (e-mail: ecmtan@ntu.edu.sg).

Digital Object Identifier 10.1109/TDMR.2003.814408

1530-4388/03$17.00 © 2003 IEEE

TABLE I
EXPERIMENTAL RESULTS TO SHOW THE EFFECT OF SUBSTRATE TEMPERATURE, CONTACT POWER AND BONDING FORCE ON THE PERCENTAGE OF ABPO

Run #	Temperature (°C)	Bond Power (mW)	Bonding Force (gf)	% of ABPO
1	115	200	20	49.51
2	215	200	55	0.10
3	215	0	20	0.00
4	125	0	20	0.98
5	215	200	20	37.25
6	115	200	55	24.80
7	125	200	55	6.47
8	115	0	20	0.20
9	215	0	55	0.00
10	115	0	55	0.00

*Sample size = 30 units/run or 1020 wires/run

TABLE II
BONDING MACHINE SETTING TO OBTAIN THE EXPERIMENTAL RESULTS SHOWN IN TABLE I

Parameters	Values
Wirebond machine	ASM AB339
Transducer Impedance	15-27 ohms
Transducer Frequency	135-138.5 KHz
Maximum Output power	800 +/- 20 mW
Product type	28Ld PDIP
Wire diameter	1 mil (Tanaka)
Capillary	Micro-Swiss P/N# 41488-0010-335 (11 mm length)
No. of Wire	34
Wire loop height	9 +/- 2 mils
1st bond time	40
1st bond force	40
Standby power	0
Contact time	10
Contact force	10
Initial bond force	20 gm
Temperature	Variable
Bond power	Variable
Bond Force	Variable

bonding is done with low power and short dwell time. In fact, the cratering damage was minimal immediately after bonding.

Comparing the above findings to our experimental results as shown in Table I, it is clear that cratering is not the root cause of ABPO, as the percentage of ABPO is lower for zero bond power than for those runs with bond power set to 200 mW. Also, there is no evidence of missing silicon or fracture at the defect site as can be seen from Fig. 1. The experimental conditions for the results of Table I are shown in Table II.

For the case of the BPSG on SiO_2, which is the case for this work, Clatterbaugh *et al.* [5] found that the best set of bonding conditions to resist cracking in BPSG films was the combination of low power, short dwell time, high substrate temperature, and high force. Their results are consistent with that reported by Koch *et al.* [6] and are also consistent with our experimental results, shown in Table I, which are extracted from the extensive design of experiments (DOE) matrices that we performed in this work.[1] Comparison of Runs 6 and 10 in Table I shows that when the bond power is reduced from 200 mW to zero,[2] the percentage of ABPO reduces from 24.8% to zero at 115 °C and 55 gf of bonding force. Also, comparison of Runs 6 and 1 shows that when the bonding force is reduced from 55 to 20 gf, the percentage of ABPO increases from 24.8% to 49.5% at 115 °C and 200 mW of bond power. Thus, one of the root causes of ABPO is cracking of the BPSG film due to the improper combination of bond power, bonding force, and temperature.

With the above-mentioned information, extensive DOE was done in order to reduce the percentage of ABPO. We found a combination of bonding power and bonding force whereby a drastic reduction in the percentage of ABPO was indeed observed. The substrate temperature is not included in the DOE as the range of variation of the temperature is limited due to the plastic casing.

With the optimal combination of the bonding power and force, the presence of ABPO remains, though at a much lower percentage. Thus, we can conclude that there is at least another root cause for the ABPO, which is very likely to be the excessive stress in the films.

[1]The complete DOE matrices cannot be shown due to confidential reasons.

[2]Although zero bond power is impractical and will cause nonstick problem, we are focused on the percentage of ABPO rather than the percentage of nonstick in the experiment.

III. FILMS STRESSES DUE TO WAFER FABRICATION PROCESSES

Smith [7] showed that the intrinsic stresses in films arise during film deposition, and their magnitudes are related to the

film microstructure and defect structure. The intrinsic stress of the metal film after all the processes is found to be as high as 770 MPa. For metal with low mobility such as W and Mo, the intrinsic stress is normally very highly tensile [8]. However, the intrinsic stress is unlikely to be one of the root causes in this work because if it is, the percentage of ABPO will be much higher, and it will occur over an entire chip rather than just a few bondpads on a chip.

For the case of BPSG, it is known that the intrinsic stress in BPSG depends on the P and B contents in the BPSG film [9]. Also, BPSG is highly hygroscopic, and it will absorb water during processing and deposition. It has been shown that it can store a large amount of water after film deposition [10]. At around 400 °C, most of the water in the film will be vaporized, which could cause delamination between BPSG and the underlying oxide. However, in our case, the bonding temperature is below 120 °C, hence, the water content should not be one of the root causes. In fact, if water content is one of the causes, a much higher percentage of ABPO will be observed as its effect will be on the entire chip as well.

Excessive fluorine in the oxide could diffuse out during BPSG anneal and cause delamination between thermal oxide and BPSG [11]. In fact, a high percentage of ABPO was observed from production lots where fluorine peak was detected using EDS on some bondpads. However, the occurrence of excess fluorine only happened twice in the six months during which the percentage of ABPO was high. Thus, the excessive fluorine is unlikely to be a root cause for ABPO.

It has also been found that the peeling stress of a film on substrate is a function of the elastic modulus, the thickness of the film and substrate [12].

Therefore, one can see that the possible root causes of ABPO that are wafer-fabrication related could be the B and P contents of the BPSG and the thicknesses of the BPSG and SiO_2. In order to examine their significance on the problem of ABPO, simulation is employed, as will be discussed later in this work.

IV. Films Stresses Due to Wire Bonding Process

Clatterbaugh *et al.* [5] found that the thin film of BPSG is not sufficiently robust to withstand any of the bonding parameters used in their studies. They found that only the combination of low bonding power, short dwell (bonding) time, high substrate temperature, and high force were able to prevent cracking of BPSG film.

In this work, many DOEs were performed to obtained the best bonding parameters such that the percentage of ABPO can be eliminated. Results showed that with the optimal bonding parameters determined, some bonding machines were indeed giving 0% of ABPO, while others showed finite number of ABPO, though the number was much reduced with the optimal setting.

Upon careful study of the differences among the bonding machines, we found that the software for the control of the bonding tool movement has the greatest effect. For a particular bonding machine, a 100-fold reduction in the percentage of ABPO was observed after a change in the software that controls the movement of the bonding tool. The change in the movement of the bonding tool with the new software is shown in Fig. 3.

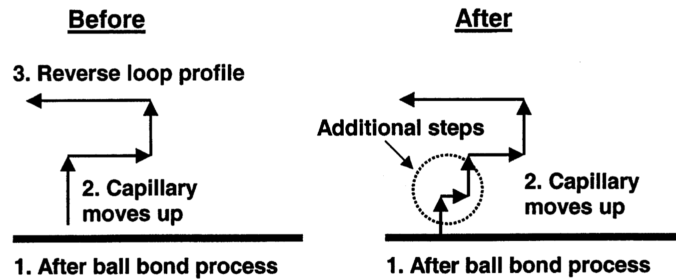

Fig. 3. Schematic illustration of the bonding tool movement before and after the software change.

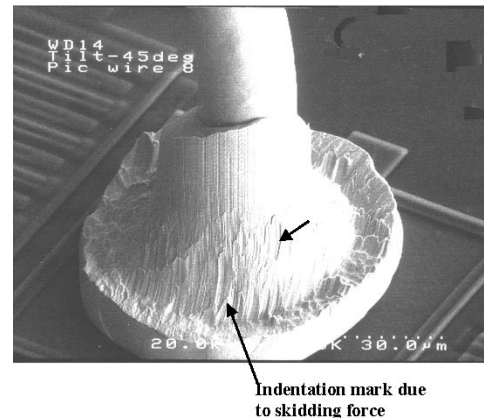

Fig. 4. Bonding ball showing skidding marks as indicated by the arrows.

On careful observation of the bonding balls, one also found obvious skidding marks on balls before the software change. The skidding marks are shown in Fig. 4. After the software change, the skidding mark becomes less obvious. Thus, one of the possible root causes will be the effect of this skidding due to the movement of the bonding tool.

V. Finite Element Analysis

Now that the various possible root causes are identified, finite element analysis is performed in order to study their effect on the stress of the BPSG layer at the BPSG/SiO_2 interface.

A schematic of the problem is shown in Fig. 5. Since the bonding ball is circular, the stress induced would be axisymmetric. Hence, by using a cylindrical structure as shown in Fig. 5 to approximate the actual structure, the simulation problem can be reduced to two dimensions.

In the analysis, all materials are assumed to be isotropic and to deform elastically. Materials properties are listed in Table III [13]–[16]. The assumption of elasticity in the simulation is justifiable, as thinner film shows much less plasticity than thick film [17]. In fact, high tensile strength is an important quality of thin films. It has been shown that the occurrence of fracture is preceded by a local plastic deformation, but at least three quarters of the deformation or elongation of the film are under elastic deformation when the film is fractured [18]. Thus, one can assume elasticity to simplify the simulation greatly.

TABLE III
MATERIAL PROPERTIES AND DIMENSIONS OF THE STRUCTURE FOR FINITE ELEMENT ANALYSIS

	Al	$MoSi_2$	BPSG	SiO_2	Si
Density (kg/m^3)	2700	2200	2590	2200	2329
Thermal conductivity (W/mK)	238	47	1	1.3376	131
Specific heat J/(Kg K)	917	816	754	816	700
Young's modulus (GPa)	67.3	225	33.2*	80	141
Poisson ratio	0.33	0.25	0.17	0.25	0.22
Coefficient of thermal expansion (K^{-1})	23.4E-6	6.79E-6	2.78E-6	1.57E-6	2.6E-6
Thickness** (nm)	1500	100*	520*	700*	500000

* These properties and dimensions are set as variables to predict their effects on the maximum shear stress.
** The radii of the materials are the same, namely, 45μm

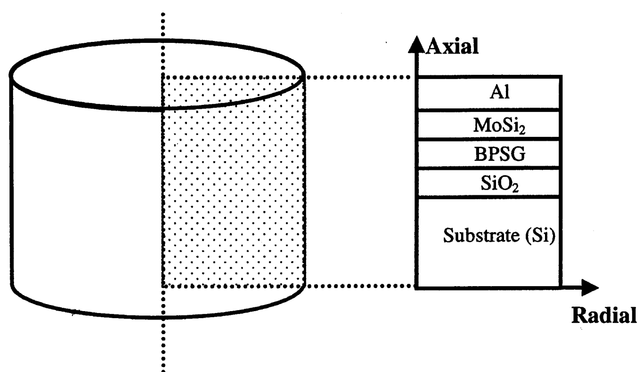

Fig. 5. Schematic graph of the cylindrical structure approximate the problem at hand (dimensions not to scale). (a) Three-dimensional view. (b) Axisymmetrical cross section.

A general-purpose finite element analysis software (ANSYS) is used for stress analysis. The element type is four-node element PLANE42. The thermal effect does not need to be considered because the temperature difference between the bondpad and the substrate is less than 1 °C [19].

Although the thermosonic gold ball bonding method is of the annular ring type, Clatterbaugh *et al.* [5] found that the stress field for an annular ring type is similar to that for a circular type of the same radius. Hence, one can further simplify the simulation by considering the circular type of the bonding ball.

A. Model Formulation

The rectangular mesh for the specimen is shown in Fig. 6. It consists of 60 columns of elements in the radial direction with 150, 5, 5, 1, and 10 rows of elements within the thicknesses (in axial direction) of Si, SiO_2, BPSG, $MoSi_2$, and Al, respectively. The location of the bonding ball is also shown in Fig. 6.

The boundary conditions used in this analysis are that the left boundary of the mesh corresponds to the axis of symmetry and therefore the displacements of all nodes at the boundary were fixed in the radial (r) direction. The bottom boundary is constrained for both radial (r) and axial (z) directions, hence, their displacement was fixed also. At the top boundary, the locations related to the contact radius are applied with a pressure corresponding to the contact force.

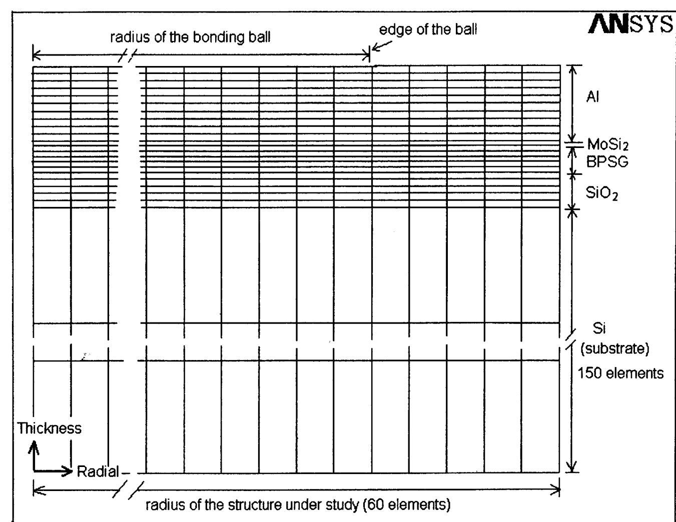

Fig. 6. Meshes of the structure for finite element analysis. The left boundary of the mesh corresponds to the axis of symmetry.

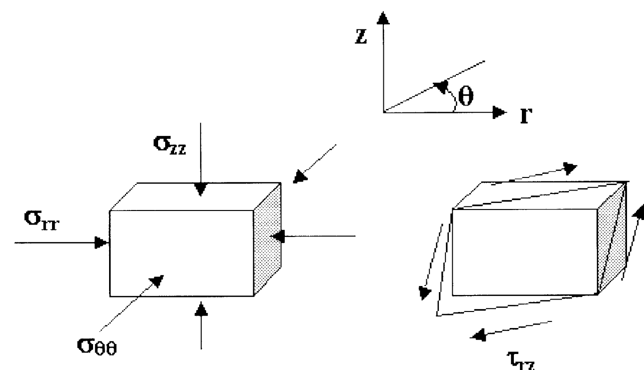

Fig. 7. Definitions of various stress components.

The various stress components computed in the simulation are defined as shown in Fig. 7.

B. Identification of the Significant Stress Component

In order to identify the most significant stress component that is responsible for the damage of the BPSG layer, we begin the simulation with the effect of bonding force as it is known that

TABLE IV
EFFECT OF B AND P CONTENTS IN BPSG ON THE PROPERTIES OF BPSG FILM AND THE SHEAR STRESS IN BPSG

B content (%)	P content (%)	Young's modulus (GPa)	Shear Stress in BPSG (MPa)
3	4	33.2	52.2
2	6	58.9	55.3

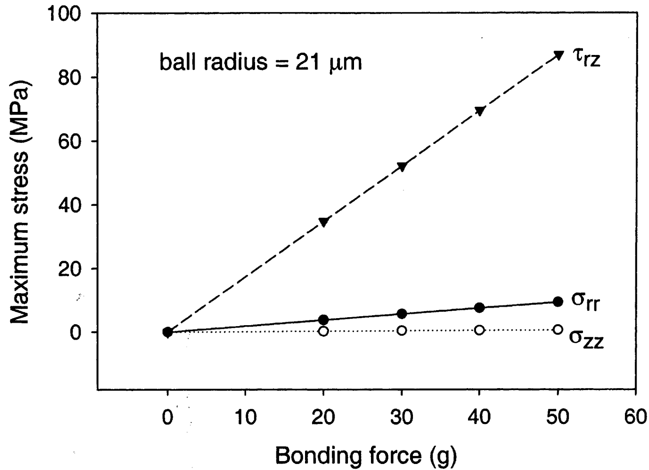

Fig. 8. Effect of bonding force on the stresses in the BPSG.

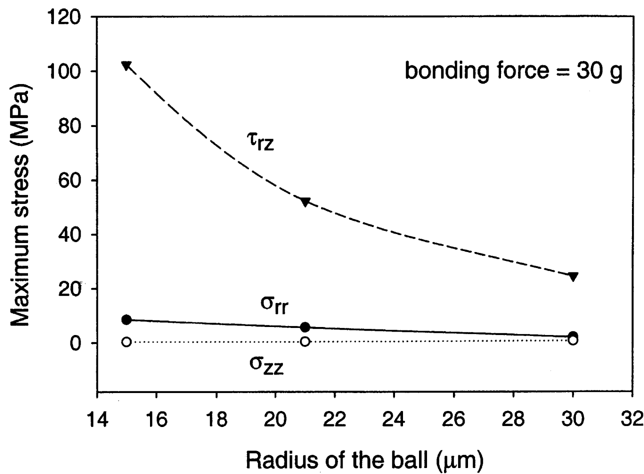

Fig. 9. Effect of bonding ball radius on the stresses in the BPSG.

bonding force has an important effect on the BPSG damage. Fig. 8 shows that the calculated shear stress (τ_{rz}) increases linearly with the bonding force, while the normal stresses (σ_{rr} and σ_{zz}) remain unchanged. The shear stress is also much higher than the normal stresses. Thus, one might conclude that the problem is due to shear stress rather than the normal stresses.

The result shown in Fig. 8 seems to be contradicted with others' work that higher bonding force is better for the BPSG layer [5]. This is because in the simulation to obtain Fig. 8, the ball diameter was assumed to be fixed. In the actual case, the ball diameter increases with the force [5]. Fig. 9 shows that the shear stress decreases drastically with the ball radius, while other stress components have relatively negligible changes. Since the decrease in shear stress with the ball radius is more drastic than the increases in shear stress due to the bonding force alone, the net result will be the decreasing shear stress as a function of the bonding force.

TABLE V
EFFECT OF BPSG THICKNESS ON THE SHEAR STRESS IN BPSG

Thickness of BPSG (nm)	Shear Stress in BPSG (MPa)
300	53.4
520	52.2
700	51.5

TABLE VI
EFFECT OF SiO_2 THICKNESS ON THE SHEAR STRESS IN BPSG

Thickness of SiO_2 (nm)	Shear Stress in BPSG (MPa)
620	52.3
700	52.2
850	52.1

From Figs. 8 and 9, one can easily see that it is the shear stress that causes the BPSG to delaminate from SiO_2, and not the other stress components. Hence, in the subsequent simulation, only shear stress is considered.

C. Effect of Wafer Fabrication Related Factors

Let us now examine the effect of the three possible root causes due to wafer fabrication processes on the shear stress in the BPSG film during wire bonding. For the contents of B and P in BPSG, they affect the Young's modulus E of the BPSG film as shown in Table IV. The ranges of B and P contents were chosen such that they covered the entire engineering specification limits for the B and P contents in the manufacturing of the wafers.

Table IV shows that this parameter does not affect the stresses for the range considered. Hence, one can conclude that the B and P contents are not critical for the problem at hand.

The next wafer-fabrication related parameters to be investigated are the thicknesses of BPSG and SiO_2. Tables V and VI show the effect of these parameters for the range of thicknesses that covered the upper and lower engineering specifications of these parameters. One can again see that these factors are not significant.

Hence, with these analysis results, one can conclude that wafer-fabrication parameters do not have significant contribution to the problem at hand.

D. Effect of Skidding

In order to study the effect of skidding, the actual skidding force has to be determined. In this work, we determine the skidding force by measuring the depth of the indentation caused by the skidding using confocal scanning laser microscopy.

Confocal microscopy has been successfully used in medical and biological applications to acquire depth or height informa-

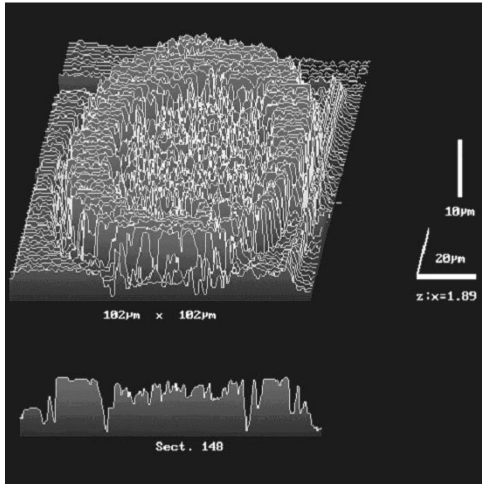

Fig. 10. Depth profile of the ball from confocal microscope (front view).

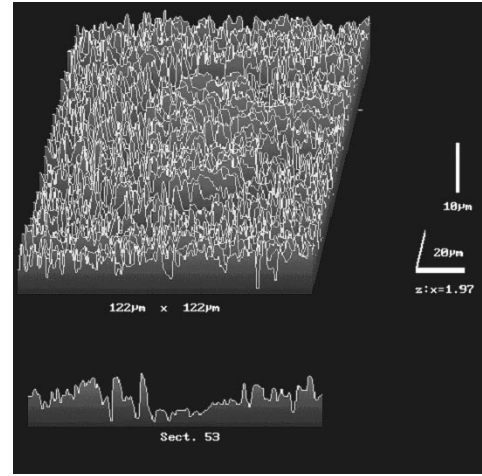

Fig. 11. Depth profile of the ball from confocal microscope (90° view) for the determination of the slope of indentation.

tion. It has also been used for fractographic analysis on die surface cracks [20]. With this microscope, three-dimensional (3-D) images and depth discrimination can be obtained [21]. For details on confocal microscopy, refer to [21].

The SEM micrograph of the ball with skidding marks was shown in Fig. 4. The corresponding depth profile as obtained from the confocal microscope is shown in Fig. 10. From the corresponding cross-sectional view, one can determine the vertical depth of the indentation.

However, since the indentation is produced on the surface of a formed bonding ball, the indentation is on a slope. Thus, the actual indentation due to the skidding force needs to be calculated using geometry, and the slope of the indentation has to be determined. Hence, we rotate the depth profile by 90° as shown in Fig. 11 to determine the slope. With the slope computed, the actual indentation can be found.

Using this method, it is found that for units with bond pad peeling, the average skidding depth is 9.6 μm. After software upgrade to reduce the skidding force, the average skidding depth is found to be 7.44 μm.

Once the indentation depth is determined, the Vickers hardness (HV) equation can be used to determine the skidding force [22]:

$$\text{HV} = \frac{1854.4P^2}{d} \tag{1}$$

where P is the force in gf, and d is the mean diagonal of indentation in micrometers [22], which can be computed from the indentation depth.

The typical HV value for the gold ball in wire bonding is 40 [23]. Since the temperature of the gold ball is at the substrate temperature, i.e., 115 °C, the HV value at 115 °C is needed. It is found that the HV for gold is not significantly sensitive to the temperature [24], hence, the HV value of 40 is used in the calculation.

With this HV value for gold, the resulting average force of skidding for units with bond pad peeling is found to be 48.7 gf, and that for units without bond pad peeling is found to be only 29.2 gf.

The induced shear stress due to skidding is then simulated using ANSYS. In this case, the structure loses its axisymmetry since the skidding force is acting only on one side of the bonding ball, and a 3-D model is necessary. However, to reduce the computational time, only a portion of the structure that includes the skidding force is considered. The size of the portion is chosen to be large enough so that further increments in size will not produce any appreciable changes in the stress distribution.

The simulated stress results showed that for units with ABPO, the shear stress in BPSG due to the skidding force is 1.73 GPa, an unexpectedly large shear stress due to skidding force. However, for units without ABPO, the shear stress in BPSG is 1.29 GPa. A difference of approximately 440 MPa in shear stress can be observed between units with and without ABPO.

From the simulation, we can see the severe effect of the skidding force. When the bonding tool movement software for all the bonding machines is upgraded, the percentage of ABPO drops to zero, indicating that skidding force is indeed the true root cause of ABPO.

VI. Conclusion

ABPO was observed with a newly developed thermosonic wirebonding process for the bonding of Au on Al bondpad in a COB assembly. Though with the use of DOE, the percentage of ABPO is much reduced with a proper combination of bonding force and power, the percentage of ABPO did not go down to zero.

With detailed failure analysis, it was found that ABPO is due to the delamination of BPSG from the underlying SiO_2 film. Many possible root causes were identified, and with the help of finite element analysis and confocal microscopy, the true root cause of ABPO is found to be the skidding force as a result of the constrained movement of the bonding tool. When the skidding force is reduced by upgrading the software that controls the bonding tool movement, the percentage of ABPO went down to zero, indicating that the true root cause for ABPO was indeed found.

ACKNOWLEDGMENT

The authors would like to thank Prof. A. K. Asundi of the School of Mechanical and Production, Nanyang Technological University, Singapore, for allowing them to use the confocal microscope for the analysis of the skidding impact, and Prof. S. Mhaisalkar of the School of Material Engineering, Nanyang Technological University, Singapore, for valuable discussions.

REFERENCES

[1] G. G. Harman, “Wirebonding—Toward 6σ yield and fine pitch,” in *Proc. 42nd Electronic Components and Technology Conf.*, San Diego, CA, May 1992, pp. 903–910.

[2] H. K. Charles Jr, K. J. Mach, S. J. Lehtonen, A. S. Francomacaro, J. S. Deboy, and R. L. Edwards, “Wirebonding at higher ultrasonic frequencies: Reliability and process implications,” *Microelectron. Reliabil.*, vol. 43, pp. 141–153, 2003.

[3] S. J. Hu, G. E. Lim, T. L. Lim, and K. P. Foong, “Study of temperature parameter on the thermosonic gold wire bonding of high speed CMOS,” *IEEE Trans. Compon. Hybrids Manufact. Technol.*, vol. 14, no. 4, pp. 855–858, 1991.

[4] Y. S. Chen and H. Fatemi, “Au wire bonding evaluation by fractional factorial designed experiment,” *Int. J. Hybrid Microelectron.*, vol. 10, no. 3, pp. 1–7, 1987.

[5] G. V. Clatterbaugh and H. K. Charles Jr, “The effect of high temperature intermetallic growth on ball shear-induced cratering,” *IEEE Trans. Compon. Hybrids Manufact. Technol.*, vol. 13, pp. 167–175, Mar. 1990.

[6] T. Koch, W. Richling, J. Whitlock, and D. Hall, “A bond failure mechanism,” in *Proc. 24th Annu. Reliability Physics*, 1986, pp. 55–60.

[7] D. Smith, *Thin Film Deposition: Principals and Practices*. New York: McGraw-Hill, 1995.

[8] J. Lee and A. S. Mack, “Finite element simulation of a stress history during the manufacturing process of thin film stacks in VLSI structures,” *IEEE Trans. Semiconduct. Manufact.*, vol. 11, pp. 458–464, Aug. 1998.

[9] H. Bouchard *et al.*, “Thermal stress in doped silicate glasses (B, P) deposited by PECVD and LPCVD,” in *Proc. MRS Symp.*, vol. 308, 1993, pp. 63–68.

[10] H. Miura and S. Ikeda, “Mechanical stress simulation for highly reliable deep-submicron devices,” *IEICE Trans. Electron.*, vol. E82-C, no. 6, p. 830, 1999.

[11] K. Ikeda *et al.*, “Water re-absorption into hygroscopic film in interlayer dielectrics and its impact on hot-carrier immunity,” in *Dig. Tech. Papers Symp. VLSI Technology*, 1996, pp. 116–117.

[12] K. Wang, Y. Huang, A. Chandra, and K. X. Hu, “Interfacial shear stress, peeling stress, and die cracking stress in trilayer electronic assemblies,” in *Proc. 7th Intersociety Conf. Thermal and Thermomechanical Phenomena in Electronic Systems*, vol. 2, 2000, pp. 56–64.

[13] J. H. Lim, J. S. Kim, K. W. Paik, and Y. Y. Earmme, “A thermomechanical analysis of MCM-D substrate of polymer and metal multilayer,” *Key Eng. Mater.*, vol. 183–187, pp. 1123–1128, 2000.

[14] T. C. Chou and T. G. Nieh, “Phase transformation and mechanical properties of thin $MoSi_2$ film produced by sputter deposition,” *Thin Solid Films*, vol. 214, pp. 48–57, 1992.

[15] F. Chen *et al.*, “Influence of underlying interlevel dielectric films on extrusion formation in aluminimum interconnects,” *J. Vac. Sci. Technol.*, vol. B18, no. 6, pp. 2826–2834, 2000.

[16] A. K. Vasudevan and J. J. Petrovic, “A comparative overview of molybdenum disilicide composites,” *Mater. Sci. Eng.*, vol. A155, pp. 1–17, 1992.

[17] R. Venkatraman and J. C. Bravman, “Separation of film thickness and grain boundary strengthening effects in Al thin films on Si,” *J. Mater. Res.*, vol. 7, no. 8, pp. 2040–2048, 1992.

[18] L. Eckertova, *Physics of Thin Films*. New York: Plenum, 1986, ch. 6.

[19] M. Mayer, O. Paul, D. Bolliger, and H. Baltes, “Integrated temperature microsensors for characterization and optimization of thermosonic ball bonding process,” *IEEE Trans. Compon. Hybrids Manufact. Technol.*, vol. 23, pp. 393–398, June 2000.

[20] M. Mohanbabu, S. Y. Khim, and E. Durai, “Fractographic analysis on the die surface crack of a LOC packaged DRAM,” in *Proc. IEEE IPFA*, 1997, pp. 224–229.

[21] T. Wilson, *Confocal Microscopy*. London, U.K.: Academic, 1990.

[22] W. D. Pilkey, “Mechanical properties and testing of engineering materials,” in *Formulas for Stress, Strain, and Structural Matrices*. New York: Wiley, 1994.

[23] G. G. Harman, “Mechanical problems in wire bonding,” in *Wire Bonding in Microelectronics: Materials, Processes, Reliability and Yield*. New York: McGraw-Hill, 1997, p. 212.

[24] V. A. Borisenko and V. P. Krashchenko, “Temperature dependences of hardness of group IB metals,” *Acta Metallurg.*, vol. 25, pp. 251–256, 1977.

Cher Ming Tan (M’84–SM’00) was born in Singapore in 1959. He received the B.Eng. degree (Hons.) in electrical engineering from the National University of Singapore in 1984 and the M.A.Sc. degree and Ph.D. degree in electrical engineering from the University of Toronto, Toronto, ON, Canada, in 1988 and 1992, respectively.

From 1992 to 1996, he was with LiteOn Power Semiconductor Corporation, Taiwan, as a Quality and Reliability Manager and an Engineering Consultant. In 1996, he joined Chartered Semiconductor Manufacturing, Ltd., Singapore, as a Quality and Reliability Section Manager. In 1997, he joined the School of Electrical and Electronic Engineering, Nanyang Technological University as a Lecturer on IC reliability and failure analysis. His current research areas include reliability data analysis, electromigration reliability physics and test methodology, silicon wafer defects study, quality engineering, and silicon-on-insulator structure fabrication technology.

Dr. Tan is currently listed in *Who’s Who in Science and Engineering* as well as *Who’s Who in the World*.

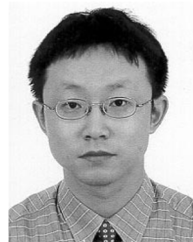

Zhenghao Gan received the B.Eng. and M.Eng. degrees in materials science and engineering from Zhejiang University, Hangzhou, China, in 1995 and 1997, respectively, and the Ph.D. degree in mechanical engineering from Nanyang Technological Uiversity, Singapore, in 2002.

He is currently a Research Fellow with the School of Electrical and Electronic Engineering, Nanyang Technological University, Singapore. His research interests include reliability and failure analysis of electronic materials and devices, and deposition and thermal-physical mechanical properties of thin films.